Study of interaction between high energy discharge and granular field in a confined environment for fuses applications

Xavier JUST[1*], Jean-Marc Chaix[1], Remy Dendievel[1], Olivier Bonnefoy[2], Gérard Thomas[2], Jean-Louis Gelet[3]

[1] SIMaP, Univ. Grenoble Alpes & CNRS, 38402, Saint Martin d'Hères
[2] LGF, ENSMSE, 158 Cours Fauriel, 42023, Saint-Etienne
[3] MERSEN, LGF, 15 rue Jacques Vaucanson, 69720, Saint-Bonnet de Mure
*xavier.just@simap.grenoble-inp.fr

Keywords: fuses, fulgurite, electrical arc, vaporization, confined media

Abstract

Industrial fuses are composed of a metallic element in compacted silica sand in a ceramic casing. In case of short circuit, rapid-heating of the metal conducts its melting and dispersion. The current is maintained momentarily by apparition of an electrical arc which create a hole of vaporized material called "arc channel". The aim of this work is to evaluate the key phenomena and variables involved in the transfer of the arc energy to the silica filler of the fuse to develop a quantitative procedure of dimensioning. The physical description is inspired by models on laser/matter interaction. Goal is to predict speeds of liquid and gas fronts, surface temperatures, and the pressure induced in the arc channel.

I. Introduction

The role of a fuse is to open the electrical circuit in case of over intensity of current, *i.e.*, when the current overcomes a predefined value. It has also to be conductive and should not significantly disturb the current in normal operating conditions.

Ultra-fast fuses are key components in protection of semi-conductors against over intensities in electrical circuits. The energy dissipated in ultra-fast fuses varies between 10^3 and 10^4 J, and the current must be cut in less than 500 µs. This energy is dissipated through an electrical arc ("arc plasma") by melting and vaporizing the medium which surrounds the conductor.

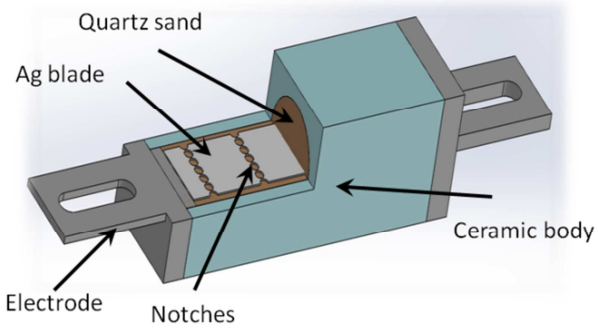

Fig.1. A typical fuse and its main components.

A typical electric fuse is made of four main components (Fig.1): the (Ag blade in the present case); the arc quenching material, usually packed silica sand [1]; the two metal electrodes which enable the contacts with the external circuit; the outer cartridge (generally a ceramic body) which ensures the mechanical and thermal protection against outer environment. The conducting/fusing part design involves the distribution of reduced sections ("notches") (Fig.2.) in which the current concentrates, and in which play the key part in fuse breaking.

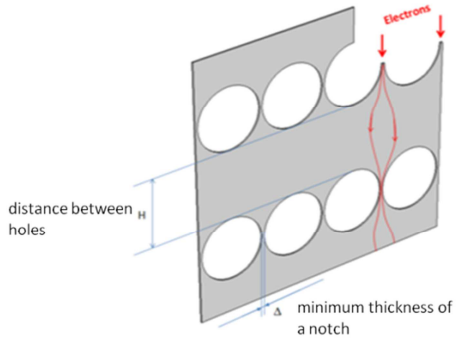

Fig.2. View of notches geometry

The events inside a fuse placed in a short circuit situation can be sequenced in three periods:

Pre-arcing period. The concentration of the high current in notches enhances the Joule effect and leads to metal melting, vaporization, and expelling of metal from the central part of the notch, leading to breaking of the conducting metal continuity. This pre-arcing period (typically 50µsec in a fast fuse) ends in the ignition of an electric arc between the two parts of the notch [2], and in the sharp increase of the voltage across the fuse.

Arcing period. The arcing period involves complex physical, chemical and mechanical aspects. General considerations about arc roots can be found in [3] and cathode and anode phenomena are reviewed in [4] with review of experimental and theoretical studies. There exist only few works on dealing with cathode and anode phenomena dedicated to electric fuses [5]. The formation and evolution of the plasma geometry and its interaction volume has been studied experimentally, with some attempts to formalize experimental results in the form of empirical models [6,7,8]. The very high gradients (temperature, pressure, electron density) from the arc channel (or core plasma) to the surrounding have strong effects on transport (electrical conductivity, radiation…) coefficients [9]. The continuous evolution of the plasma composition was discussed on the basis of physical and chemical considerations [10], leading to typical temperatures around 20 000 K. During this arcing period, an erosion of the fuse element at the ends of the arc occurs. This *burn-back* phenomenon has been widely studied within the electric fuse community [7]. The produced liquid and vapor silver is expelled through the porosity of the surrounding silica sand medium. The energy production from the arc also melts and vaporizes the surrounding silica, leading to the typical geometry presented on Fig.3, in which the arc channel containing the plasma is bounded by solid and melted silica.

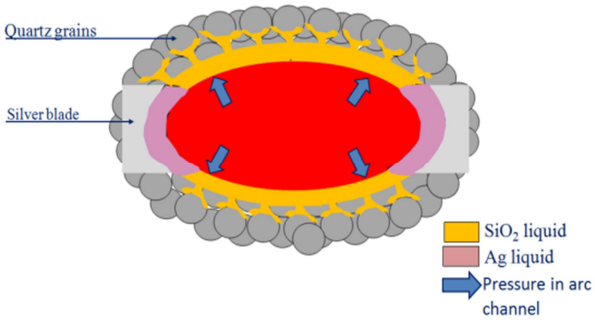

Fig.3. Schematic view of the arc channel during the arcing period: the arc between the silver electrodes is confined in a volume bounded by liquid silica and silica packed sand.

Post-arcing period. Once the arcing period is ended, the quartz structure is quenched and the solidified silica leads to a solid arc channel or lumen (Fig.3). The extreme and rapid processes of heating and cooling results in the formation of silica glass, the so-called lechatelierite, which exhibits typical flow structure and vesicles. The obtained structure reminds what is observed when lightning interacts with sand and form a glassy and rooty tube (fulgurite, from latin *fulgur*, lightening). This structure has to ensure high dielectric rigidity to prevent restriking, and was studied [12] because of this high industrial interest.

The present work explores the arcing period, in the case of ultra-fast fuses. Its main goal is to propose a first description of quartz sand behavior under specific conditions involved in these high speed fuses. Most of the published works aim at predicting current and voltage induced by the fuse[8]; they are generally depending on fitting parameters (type of fuse or geometrical considerations). Physical modeling in fuses was proposed in some cases, *e.g.*, to account for gas flow and heat transfer of fluid in the porous medium [13]. This paper focuses on the interaction between electrical arc and the surrounding quartz sand, which drives the evolution of the arc channel during the arcing period. The electrical arc is considered as a heat source and the compacted sand as

an equivalent porous medium. Because of the characteristic time and dissipated power, the proposed model is based on laser/matter interaction works on laser drilling. The power input and geometric conditions are deduced from experiments and observations.

II. Methodology

1. Experimentals

Due to the very high velocity of the involved phenomena (200µsec), and to the fact that they occur inside a closed box in an opaque medium, *in situ* observations are not possible. The experimental data acquisition therefore involves two approaches.

The first approach is a macroscopic analysis of electrical analysis of the behavior of the fuse when placed in a short-circuit reference situation. The tension *U(t)* and current *I(t)* are recorded. These experimental curves (Fig. 4) clearly show the pre-arcing period (Joule heating of the Ag before melting and expelling) at low voltage, and the abrupt increase of voltage when the silver continuity is arc is formed. The product *U(t).I(t)* energy absorbed by the fuse per unit time is drastically increased when the arc forms. From this product and the number of notches in the fuse, it possible to calculate the power dissipated in the granular field in each notch.

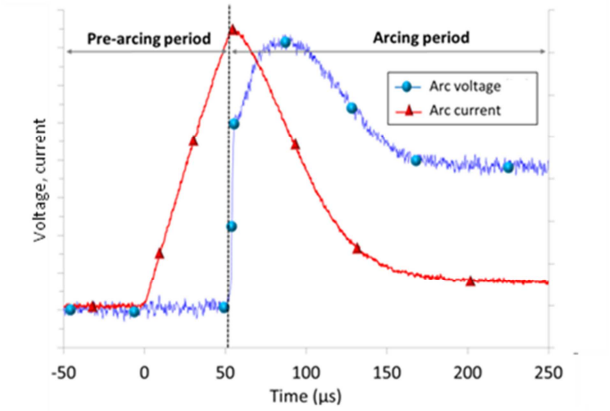

Fig.4. Typical evolution of tension and current during fuse breaking

The second approach is the observation of the corresponding fuses at microscopic scale. Two techniques were used:

- Observation of polished cross sections of small blocks (a few mm) around notches extracted from broken fuses. The blocks were impregnated by an epoxy resin, then cut, polished and observed in a Scanning electron Microscope (SEM).
- Observation of such blocks by X-ray microtomography. This technique enables non-destructive 3D analysis of materials microsctucture [14,15]. Microtomography experiments were performed on a a microtomograph Easy Tom XL150, using 2.5 µm voxel size. It was possible to separate SiO_2, Ag and pores from grey levels.

The use of these two techniques leads to qualitative observations and quantitative evaluation of characteristic sizes.

2. Model

Basic assumptions and simplifications

This model aims at evaluating the evolution of the arc channel after the arc is formed. The arc channel is modeled as a cylinder filled of high temperature gas. The arc is considered as a linear power source along the channel axis. The power of this source per unit length of arc channel is an input, obtained from electrical measurements (see previous paragraphs). The cylinder is surrounded by the porous silica medium constituted by compacted sand and typically 50% interparticle pores. The heat flow from the arc heats the side surface of the cylinder (heat exchanges at the ends along the axis are neglected). Heat is dissipated by diffusion inside the porous medium, melting and evaporation of silica. The arc length is assumed constant (*i.e.* the burn back phenomenon is assumed rapid). The arc channel radius *r* expands by melting and evaporation of silica. This allows using a 1D-axisymetric model.

Silver is not taken into account in this first approach for two main reasons, deduced from observations (see results of broken fuses observation): i) most of the fused metal Ag blade is expelled backwards outside the channel area during the burn-back phenomenon, ii) the corresponding metal mass is typically 2.3mg and a simple evaluation of the energy needed to heat and melt shows that it only uses 15% of the overall input energy per notch (6J out of 20J). The presence of Ag in the arc plasma is of course significant, but the present model doesn't aim at understanding the plasma, and considers the power as an input.

The power flux from the arc per unit area of cylinder is:

$$\varphi_{arc}(t) = \frac{P_l(t)}{r(t)} \qquad (1)$$

where $P_l(t)$ is the power flux per unit length of arc channel

Heat transfer in the silica porous medium

Considering the velocity $u=dr/dt$ of the arc channel surface, the conduction through the silica medium writes:

$$C_p\rho(T)\left[\frac{\partial T}{\partial t}+\ \nabla.(u.T)\right]=\nabla.k(T)\nabla T \qquad (2)$$

where ρ is the density of condensed phase (kg/m^3), k the thermal conductivity (W.m/s), T the temperature (K), and C_p the heat capacity per unit mass (J.K^{-1}.Kg^{-1}).

The melting of silica is taken into account through a continuous description by replacing C_p in eqn.(11) by a the pseudo-heat capacity:

$$C_p^*(T)=C_p(T)+\frac{e^{-\frac{(T-T_m)}{\Delta T^2}}}{\Delta T\sqrt{\pi}}L_m \qquad (3)$$

with T_m the melting point, ΔT an arbitrarily chosen melting temperature interval (ΔT=10K was used here), L_m the enthalpy of melting.

Boundary condition at the SiO_2-channel interface

The energy balance at the channel surface is:

$$\varphi_{arc}(t)-\dot{m}_{vap}.L_v-k\nabla T=0 \quad (4)$$

where L_v is the enthalpy of vaporization and $\dot{m}_{vap}$ the mass of silica evaporating per unit time per unit surface.

The evaluation of $\dot{m}_{vap}$ is the key point of the model. The classic Hertz-Knudsen-Langmuir equation , which is used in problems such as laser drilling [16] which involve similar heat fluxes and typical times was applied. This equation describes the evaporation velocity of a molecular compound. A simple formulation is:

$$\dot{m}_{vap}=\ (1-\beta_r)\ \left(\frac{M}{2\pi RT_S}\right)^{1/2}P_{sat} \qquad (5)$$

where M is the molecular mass, R the gas constant, P_{sat} the equilibrium vapor pressure (saturation) at the liquid-gas surface at temperature T_s.

Coefficient β_r depends on both the total pressure in the gas and the partial pressure of the evaporating compound. It is 0 when the evaporating phase is maintained in vacuum (*i.e.* when the gas pressure is low), equal to unity when the partial pressure of the considered compound is equal to P_{sat}, and larger than unity (condensation) for higher partial pressures.

In the present model, silica is assumed to evaporate without dissociation, or at least that the saturation pressure concept can be applied, and that the classic Clausius-Clapeyron can be used. This equation allows the calculation of P_{sat} as: describes the change of equilibrium vapor pressure as function of temperature and is given by:

$$\frac{1}{P_{sat}}\frac{dP_{sat}}{dT}=\frac{\Delta H_{vap}}{RT^2} \qquad (6)$$

where ΔH_{vap} the enthalpy of vaporization and R is is the molar gas constant. If, ΔH_{vap} is assumed constant in the temperature range of interest, this leads to:

$$P_{sat}(T)=P_{sat}^0e^{-\frac{\Delta H_{vap}}{R}\left(\frac{1}{T}-\frac{1}{T_0}\right)} \qquad (7)$$

with T_0 the boiling temperature at pressure: P_{sat}^0 ,*i.e.*, in the case of silica T_0=3200K at P_{sat}^0=10^{5}Pa

Substituting eqn.(7) into eqn.(5) for vaporization rate yields:

$$\dot{m}_{vap}=\ \left(\frac{M}{2\pi k_BT_S}\right)P_{sat}^0e^{-\frac{\Delta H_{vap}}{R}\left(\frac{1}{T_S}-\frac{1}{T_0}\right)}(1-\beta_r) \qquad (8)$$

Coefficient $\beta_r$cannot be determined. We therefore selected two extreme cases:

$$\beta_r=0 \quad (9)$$

which should describe the evolution when the SiO_2 pressure in the channel remains small. This can be a valid approximation when the silica vapor escapes through the porous sand packing.

$$\beta_r=\frac{P_{SiO2}}{P_{sat}(T)} \qquad (10)$$

with *P* the total pressure, which accounts for the inhibition of evaporation by the gas, and. This is particularly significant when most of the evaporated silica remains in the arc channel (note that here *P* is close to the partial pressure of silica).

Pressure in the arc channel

The pressure evolution in the arc channel depends on whether the gas can escape or not. When the gas easily escapes (open system) the pressure remains constant, and relatively low.

If the gas cannot escape, which will occur for instance if the melted silica forms a continuous liquid layer around the arc channel, the pressure in the channel will increase as evaporation progresses. In this case, the pressure was evaluated at each time *t* using the perfect gas law:

$$PV = n_g RT_S \qquad (11)$$

in which the number n_g of moles in the channel and the volume *V* of the channel are calculated from the time integration of $\dot{m}_{vap}$ from 0 to *t*. The gas temperature is assumed to be equal to the temperature surface T_s.

Numerical implementation

Computer simulations were realized using the finite element method (FEM) by means of the Comsol Multiphysics® software package. This package includes an ALE (Arbitrary Lagrangian Eulerian) technique [17] which enables tracking the liquid gas interface and taking it into account in the heat diffusion equations, with this moving boundary without remeshing.

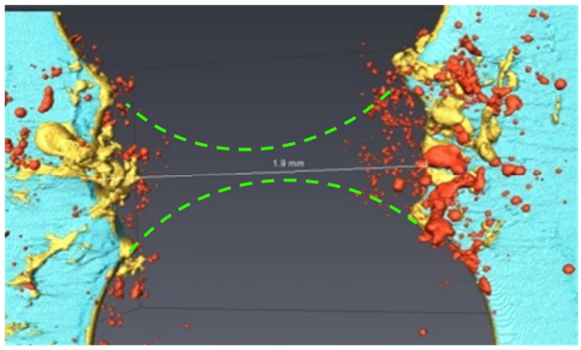

Fig.5. 3D distribution of silver around a former notch. The unaffected part of the silver blade is in light blue; the red and yellow objects are solidified Ag drops expelled out from the notch by the arc and by the burn back phenomenon. The yellow ones are in contact with the blade. The green dashed curve marks the initial Ag notch.

III. Results

Used fused observation

Ag notches

The distribution of Ag in a used fast fuse around a former notch is presented on Fig.5. On this 3D X-ray tomography image, the sand was made transparent to observe the 3D distribution of silver (Fig.5.). During the burn back phenomenon most of the silver was expelled away, mainly backwards (towards the Ag blade), so that almost no silver remains in the silica sand close to the arc channel. This dispersion can also be seen on SEM images of cross section (Fig.6). The measurement of the melted volume of the notch on 3D images (green bounds on fig. 5) shows that 2mm^3 of silver were melted and expelled.

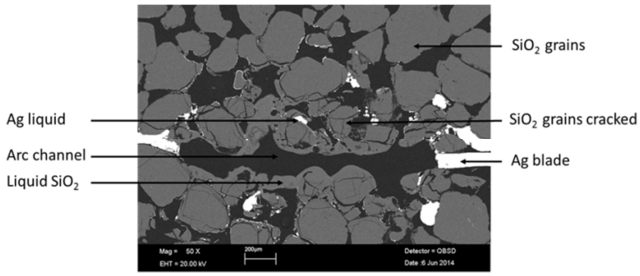

Fig.6. SEM image of the cross section (perpendicular to the silver blade) of the arc channel in a used ultra-fast fuse.

Arc channel

The SEM images of arc channel cross sections (Fig.6) show the melted silica at the internal boundary of the arc channel, due to the absorption of the arc energy. The observation of the 3D distribution of glassy silica was not possible, due to the too low contrast between amorphous and crystalline (quartz) silica in microtomography images. Quantative analysis of the 3D microtomography images were used to evaluate the volume melted Ag and geometric characteristics of the arc channel, such as the arc channel length and volume (Table 1).

Cracks through the grains are also observed clos to the arc channel boundary (Fig.5), but their origin is an open question: shock wave during the arc or thermal shock during quenching?

Arc channel volume ("empty" volume)	1 mm^3
Volume of fused and dispersed silver	0.2 mm^3
Former sand+pore volume	0.8 mm^3
Arc channel length	2.3 mm
Equivalent radius of the arc channel radius	0.37mm
Melted silica layer width	100 to 200 µm

Table 1. Typical arc channel geometric characteristics obtained from SEM and XRay microtomography images

Modeling

Input data

The physical characteristics of the porous silica sand medium (porosity around 30%) are summarized in Table2. The length of the arc channel is h_0 = 2.3 mm (Table 1). Its initial radius is set equal to the initial radius of a notch i.e. r_0 = 100 µm.

Parameters	Symbol [Unit]	Value [transition at T_{fus}]
Room temperature	T_R [K]	293
Melting point	T_m [K]	1996
Melting latent heat	L_m [$J.kg^{-1}$]	$1.595\ 10^6$
Evaporation latent heat	L_v [$J.kg^{-1}$]	$8.87\ 10^6$
Heat capacity (solid)	C_p[$J.kg^{-1}.K^{-1}$]	765
Heat capacity (liquid)	C_p[$J.kg^{-1}.K^{-1}$]	1426
Heat conductivity (s)	k [$W.m^{-1}.K^{-1}$]	0.33
Heat conductivity (l)	k [$W.m^{-1}.K^{-1}$]	5
Packed sand density	ρ [$kg.m^{-3}$]	1700
Liquid silica density	ρ [$kg.m^{-3}$]	2100

Table 2. Physical data used in computations for the porous silica medium.

The evolution of arc power per unit length of arc channel obtained from macroscopic measurements of tension and current is presented on Fig. 7: the power rapidly increases in the first microseconds, reaches a maximum value after 30µsec, and then drops by a factor of 1000 after 60 to 80µsec.

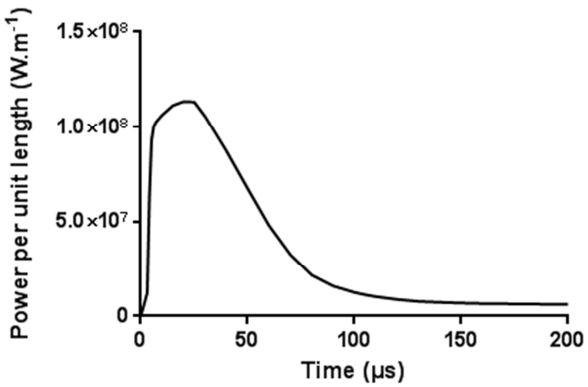

Fig.7. Time evolution of the power (W/m) dissipated by the arc per unit length of arc channel, calculated from

Résults

Three examples of outputs are presented on Figs. 8 to 10, with the coefficient β_r being set to zero or depending on the pressure pressure in the arc channel.

The evolution of the width of vaporized silica ("vaporized radius" on Fig.8) rapidly increases, to reach values around 250µm. This corresponds to about 0.3 to 0.4 mm^3 around each notch. This value is about half the volume deduced from arc channel measurements (0.8 mm^3, Table 1): the difference could be explained by the flow of melted in the pores, which is not taken into account in the model. The total evaporated volume is lower when the increase of β_r with pressure is considered: this is due to the limiting effect of pressure on the vaporization rate. The decrease of the vaporized volume after 100µsec when $\beta_r = \frac{P_{SiO_2}}{P_{Sat}}$ corresponds to the condensation of the confined vapor when the arc power ends, while the model with $\beta_r = 0$, which corresponds to an open system in which silica vapor went out, leads to a constant vaporized radius.

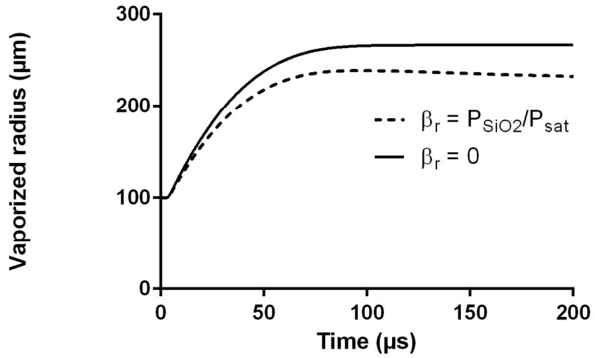

Fig.8. Computed evolution of the vaporized radius Δr = r-r_0 for $\beta_r = \frac{P_{SiO_2}}{P_{Sat}}$ *and* $\beta_r = 0$

The evolution of temperature T_s at the surface of silica facing the arc channel (Fig.9) shows a drastic increase in the first microseconds, which simply corresponds to the fast increase of the power (Fig.7). Strong differences are however observed between the $\beta_r = 0$ case and when β_r depends on pressure. When $\beta_r = 0$, the maximum temperature, around 5000K, decreases after a few microseconds: the decrease of the heat flux φ_{arc} towards the surface due to the increase of the channel radius (Eqn. 1) overcomes the increase of the power flux P_l. When the arc power ends is around, temperatures tends to about 2000K, which corresponds to the 'slow' solidification of the liquid layer.

In the case of the pressure dependant β_r, a higher temperature is reached (8500K), and the decrease after a few microseconds is not observed, because the increasing pressure shifts the temperature towards higher values. The maximum temperature remains high when the arc power ends: in this case, gaz condensation is observed ($\beta_r > 1$), with the high pressure-high pressure gaz as energy and matter source.

It is to be noticed that the predicted surface temperatures are high but remain below the values expected in the arc plasma.

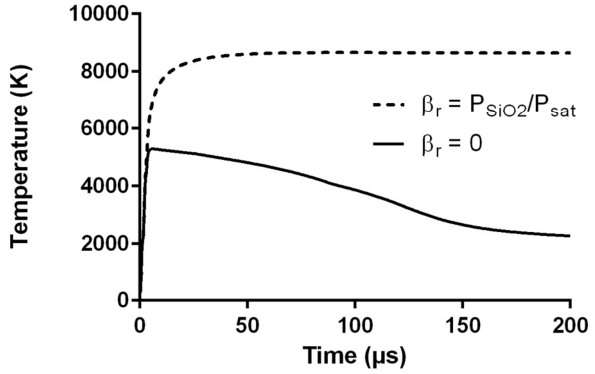

Fig.9. Evolution of surface temperature in case of $\beta_r = \frac{P_{SiO_2}}{P_{Sat}}$ *and* $\beta_r = 0$

The evolution of internal pressure of SiO_2 in the arc channel calculated for a closed channel is presented on Fig.10. The high values (1-2GPa) reached in both cases clearly show that the $\beta_r = 0$ case is not compatible with a closed channel, and must be used only.

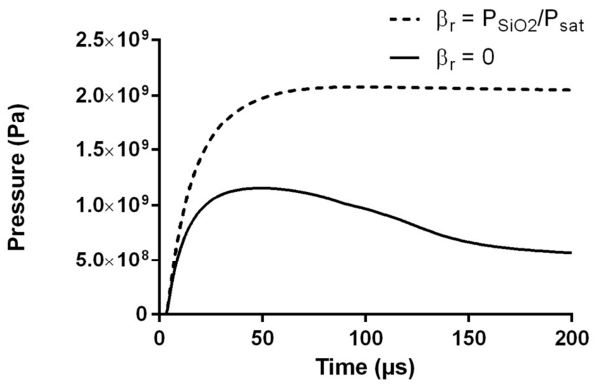

Fig.10. Evolution of pressure in case of $\beta_r = \frac{P_{SiO_2}}{P_{Sat}}$

The partial pressure reaching 1-2 GPa in 10 µs is very high. Saquib and Stockes [18] used mechanical sensors to measure the pressure during arc extinction. They obtained maximal values during the arc extinction between 1.6 MPa for a current of 1 kA to 5.5 MPa for a current of 4 kA. However, the sensors were placed at 10 mm from the core of the arc, i.e. at the edge of a volume about 103 times larger than the present arc channels. In high speed fuses, the maximum current is 60 kA and because of the very small involved volumes between notches, we can suppose that the values reached in the arc column is far higher.

4. Conclusions

The simple model presented here is based on experimental observations and data, without any adjustable parameter. It leads to correct orders of magnitude of the amount of vaporized matter. It also provides estimations of temperature on the liquid/gas interface and pressure in the arc channel.

The obtained temperatures are below the typical plasma temperatures expected in arc plasmas (20 000K) [9] arc and they can be considered acceptable as liquid/gas interface temperature.

In the light of results on pressure in the arc channel (rapid increasing and high final value around 1 GPa) two phenomena should be taken into consideration: i) because of the porosity of the granular field a part of the gas and liquid propagate in granular field, ii) due to very quick increasing of the pressure a shock wave could be transmitted through the solid.

Additional experimental data have to be collected during arcing, (pressure and temperature), although they are hard to obtain because of the extreme conditions (high temperature, closed field…). X-ray tomography will give other orders of magnitudes on ablated material for different characteristics (U and I) and the amount of fused silica. Thermochemical data on the system Ag-SiO_2 could help understanding the phenomena and estimating kinetics and temperatures.

5. Acknowledgements

This work is part of the FE^2E project supported by the FUI-AAP15 program of the French Government.

6. References

[1] Bussière, W.: ‘Electric fuses operation, a review: 1. Pre-arcing period’ (IOP Conf. Ser.: Mater. Sci. Eng. , 2012)

[2] Memiaghe, S.: ‘Modélisation du régime de préarc dans les fusibles’ PhD thesis, Université Blaise Pascal, Clermont-Ferrand, France, 2010

[3] Abbaoui, M., Lefort, A.: ‘Arc root interaction with the electrode: a comparative study of 1D-2D axi symmetric simulation’, Euro. Phys. J. Appl. Phys., 2009, 48, N°1 11001

[4] Benilov, MS.:’Theory and modeling of arc cathodes’, Plasma Sources Sci. Technol., 2002, 11, pp. 49-54

[5] Gnanalingham, S., Beaumont, KJ.: ‘Digital simulation of fuse breaking test’. Proc. IEE., 1980, 127 C 6, pp. 434-44

[6] Wright, A., Beaumont, KJ.: ‘Analysis of high-breaking-capacity fuselink arcing phenomena’, Proc. IEE., 1976, 123, pp. 252-258

[7] Sloot, JGJ,. Kalasek, VKI., Sikkenga, J. : 'A one dimensional mathematical model for the dynamic burnback velocity of silver strips'. Proc. Of the 3rd Int. Conf. on Electric Fuses and their applications, Eindhoven, Netherlands, 1987, pp. 72-77

[8] Daalder, J A., Schreurs , EF.: 'Arcing phenomena in high voltage fuses' , EUT. report., 1983, 83-E-13

[9] Bussière, W., André, P.: 'Evolution of the composition, the pressure, the thermodynamic properties and monoatomic spectral line at fixed volume for $SiO_2 - Ag$ plasma in the temperature range 5000-25000 K' J. Phys. D: Appl. Phys., 2001, 34, pp. 1657-1664

[10] Bussière, W.: 'Mesure des grandeurs (T, Ne, P) au sein du plasma d'arc des fusibles en moyenne tension'. PhD thesis, Université Blaise Pascal, Clermont-Ferrand, France, 2000

[11] Cwidak, K., Lipski, T .: 'New results on post arc fulgurite resistance of HBC fuses'. Proc. Int. Conf. On Electric Fuses and their Applications (ICEFA), Ilmenau, Germany, May 1995, pp. 223-228

[13] Rochette, D., Clain, S.: 'Mathematical model and simulation of gas flow through a porous medium in high breaking capacity fuses' IET J. of Heat and Fluid Flow., 2004, 53, pp 25-37

[14] Baruchel, J., Buffière, J.Y., Maire, E., Merle, P., Peix, J. : 'X-Ray Tomography in Material Science' (Hermès, 2000)

[15] Salvo, L., Cloetens, P., Maire, E., Zabler, S., Blandin, J.J. , Buffière, J.Y., Ludwig, W., Boller, E. , Bellet, D., Josserond, C. : 'X-ray micro-tomography an attractive characterisation technique in materials science' Nuclear Instruments and Methods in Physics Research 2003, B 200, pp 273–286

[16] Anisimov, SI., Khokhlov,A.: 'Instabilities in Laser-Matter Interaction', (CRC Press, 1996)

[17] Touvrey, C., Bruyere, V., Namy, P.: 'Comparison between Phase Field and ALE methods to model the keyhole digging during spot laser welding'. Proc. Int. Conf. Comsol Conference, Rotterdam, Netherland, September 2006, pp. 1-7

[18] Saqib, M A., Stokes, A D., and Seebacher, P J.: 'Pressure inside the arc channel of a high-voltage'. Proc.Int. Conf. on Electric Fuses and their Applications, Torino, Italy, September 1999, pp. 83–89